Development of the lumped parameter core makeup tank model of SMART and assessment using the SPACE code

Min Gi Kim[a], Adnan Wisudhaputra[a], Jae Jun Jeong[*a], Jong-Hyuk Lee[b], Kyungdoo Kim[b], Hyun-Sik Park[c]
[a] *School of Mechanical Engineering, Pusan National University (PNU)*
[b] *Virtual Nuclear Power Plant Technology Development Division, Korea Atomic Energy Research Institute (KAERI)*
[c] *Innovative System Safety Research Division, Korea Atomic Energy Research Institute (KAERI)*

[*] *Corresponding author: jjjeong@pusan.ac.kr*

1. Introduction

The SMART reactor [1] has various passive safety systems. For example, PSIS (Passive Safety Injection System) contains CMT (Core Makeup Tank) and SIT (Safety Injection Tank) for core cooling and coolant replenishment. For the assessment of PSIS performance, some integral effect tests [2] have been carried out with integral effect facility, SMART-ITL [3]. Recently PNU has simulated the experiments for model development and validation of the thermal-hydraulic code, SPACE. It was shown that the SPACE code did not properly calculate the performance of the PSIS. This was because the SPACE code uses the bulk liquid temperature to calculate the interfacial heat transfer between water and the interface, so the overall interfacial heat transfer was over-predicted. In this paper, we developed a lumped CMT model that can calculate the interfacial heat transfer realistically. The new model was based on a lumped-parameter model assuming the simplified liquid temperature distribution. Then, we assessed the CMT model using the PSIS performance tests. The results showed that the CMT model predicts the behaviors of the CMT and SIT reasonably well. Future improvements were specified.

2. Preliminary simulation of the PSIS performance experiments

2.1 Test facility and test scenario

SMART-ITL [3] is a thermal-hydraulic integral effect test facility for SMART. This facility is scaled with a full height, and 1/49 volume and power scale. The primary system consists of a reactor pressure vessel, a two-stage automatic depressurization system (ADS), and four trains of passive safety injection system (PSIS). the secondary system has four steam generators and four trains of passive residual heat removal system (PRHRS). Fig. 1 shows a schematic of the SMART-ITL [4].

In detail about PSIS, PSIS has 4 trains. In each of the PSIS trains, there is one CMT and SIT per train. The pressure balance line (PBL) is connected between the top of the CMT and the RPV. The PBL balances the pressure between them. When the CMT injection starts, the valve at the bottom of the CMT is opened and water is injected into the RPV through the safety injection (SI) line. The SIT maintains nearly atmospheric pressure while being closed by valves. Also, at the bottom of SIT, a check valve is located to prevent reversed flow.

Recently, series of tests [2] were performed to test performances of passive safety systems in various accident conditions. Among the tests, F101 and F102 are the PSIS performance test. Each test focused on the behaviors of CMT and SIT in the SBLOCA condition. In both experiments, KAERI set the SBLOCA condition by assuming a 2-inch break at the SI line. The break nozzle is in one SI line which is the same elevation with upper downcomer (UDC) and RCP. The location of the break is shown in Fig. 2.

The major sequence [5] is shown in Table I. In the F101 and F102 tests, once a break occurred, RCS pressure decreases as the coolant discharges through the break. When the pressurizer pressure reaches a low PZR pressure setpoint (LPP), a reactor trip signal is generated with 1.1 second delay. As assuming a turbine trip, RCP coast down, and FW stop signal occurs at the same time with reactor trip signal, a core makeup tank actuation signal (CMTAS) is generated coincidently. Decay heat starts after LPP with 1.6 second delay. CMT injection starts following the CMTAS with 1.1 second delay. passive residual heat removal actuation signal (PRHRAS) is generated after LPP with 5.2 second. MSIV and FIV are closed after PRHRAS with 5.0 second time delay. When the pressurizer pressure reaches the safety injection tank actuation signal (SITAS) setpoint, SIT injection starts following the SITAS with 1.1 second delay. In both experiments, four trains of PRHRS are not available. Also, because one SI line was assumed as break location, only 3 trains of the PSIS are available. The F101 test allows CMT injection only while the F102 test allows SIT injection only.

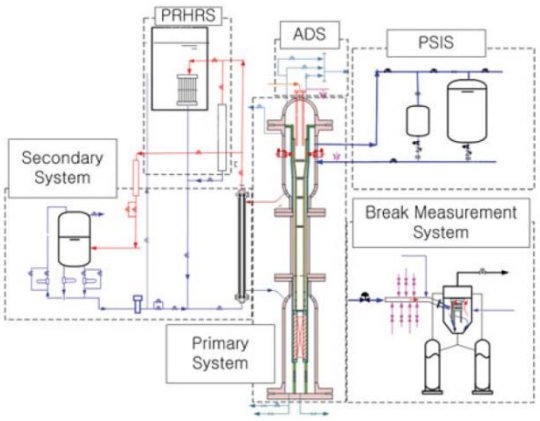

Fig. 1. Schematic of SMART-ITL (simplified) [4].

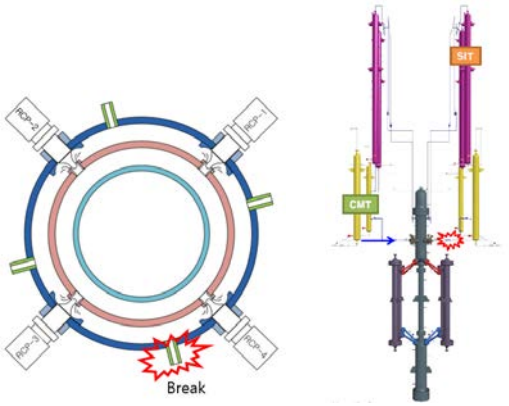

(a) Top view of UDC (b) Axial view of SMART-ITL

Fig. 2. Break location.

Table I: Major sequence of events for the SBLOCA scenario

Event	Trip signal and set point
Break	
LPP setpoint	PZR Pressure = P_{LPP} (10.26 MPa)
LPP reactor trip signal	LPP + 1.1 s
Turbine trip RCP coastdown FW stop CMTAS is generated	
Control rod starts to drop	LPP + 1.6 s
CMT injection start	CMTAS + 1.1 s (LPP + 2.2 s)
PRHRSAS generation	LPP + 5.2 s
MSIV/MFIV close	PRHRAS + 5.0 s (LPP+10.2 s)
SITAS generation	PZR Pressure = P_{SITAS} (2.0 MPa)
SIT injection starts	SITAS + 1.1 s

2.2 SPACE modeling

A nodalization of SMART-ITL is shown in Fig. 3. For the simulation, the reactor coolant system, three trains of PSIS including SIT and CMT, and secondary side four steam generators are considered. Because the decay power was not considered in both experiments, decay power was entered as following the measured heater power. For pump modeling, homologous curves for the installed RCPs were used. The operation logics for steady-state calculation are considered at each device such as RCP, FW, etc.

Heat structures are attached to each node considering geometrical information and material property. Heat transfer correlations at SGs are used as default correlations of the SPACE code. The heat loss was considered by the implementation of boundary conditions, the outside temperature air temperature and heat transfer coefficient, in the heat structure which is attached to the RPV.

For break modeling, we attached TFBC component at the upper downcomer (UDC) which is same elevation with RCPs. We used Henry-Fauske model using the discharge coefficient as default value (1.0). In this nodalization, UDC modeling is considered by dividing as 8 sections. Fig. 4 shows the break part modeling.

The PSIS modeling is shown in Fig. 5. The CMT and SIT of PSIS are implemented as PIPE components of 12 nodes each. The orifices installed in each PBL and SI were implemented with loss coefficients. The valves used for CMT and SIT operation are implemented as trip valves to open under operating conditions. In this calculation, heat structures are not considered in the PSIS to exclude the wall effect on the PSIS injection behaviors.

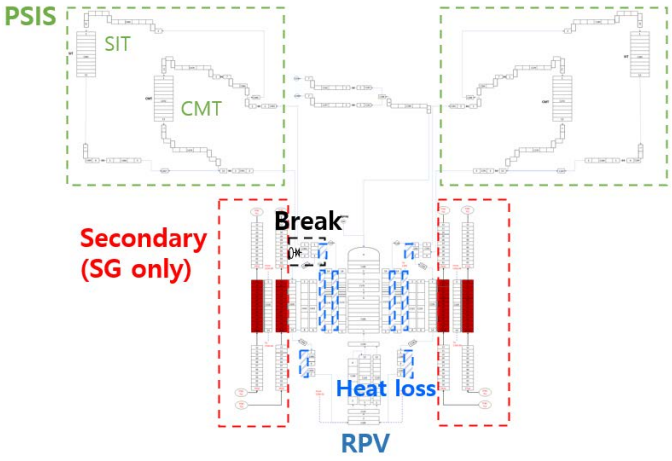

Fig. 3. Nodalization of SMART-ITL for SPACE (for clear representation, only two rains of PSIS are displayed).

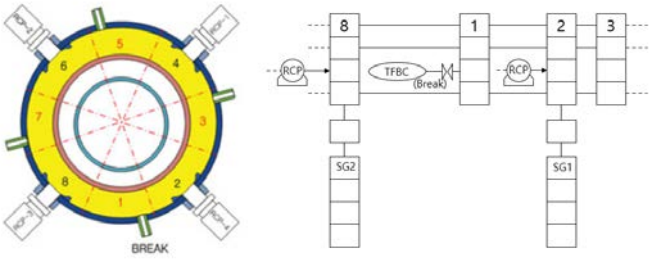

(a) Top view (b) Axial view

Fig. 4. Representations of the UDC and break modeling.

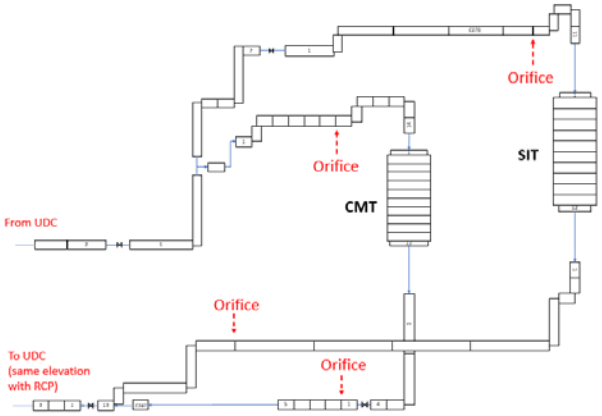

Fig. 5. Nodalization of PSIS.

2.3 Steady-state results

Table II represents the results of steady-state calculations which are normalized by measured value. In both experiments, because the RCS flow was under-measured, the RCP was controlled by targeting the mass flow suitable for the actual thermal equilibrium between the core power and SG heat removal. Therefore, the RCS flow in the calculation was over-predicted compared to the experiment. Overall, both results show that the calculations well followed the experimental conditions.

Table II: Normalized steady-state calculation result

Parameter	Calculated value / Measured value	
	F101	F102
Core power	1.0	1.0
PZR power	-	-
Core outlet/inlet temperature	1.0 / 1.0	1.0 / 1.0
Hot leg / Cold leg temperature	0.99 / 0.99	0.99 / 0.99
RCS flow rate	1.11	1.10
PZR pressure	1.0	1.0
PZR temperature	1.0	1.0
PZR water level	1.0	1.0
SG inlet / outlet temperature	1.0 / 1.01	1.0 / 1.01
SG flow rate	1.0	1.0
Feedwater / Main steam pressure	0.99 / 1.0	0.99 / 1.0

2.4 Transient results

Figs. 6 to 10 show the calculated values of main parameter behaviors compared to the experiment in the F101 simulation. Both results were normalized. Fig. 6 shows the measured and calculated power after the reactor trip. The decay power entered in the input deck well follows the measured value in the experiment. As shown in Fig. 7, pressurizer pressure was decreased after the break. In the calculation, the LPP signal was slower and the accumulated break flow was larger than the F101 experiment (Fig. 7 and Fig. 8). Fig. 9 shows the total mass flow rate of four cold legs.

However, a more important problem was in the PSIS. Fig. 10 shows the mass flow rate of the first train SI line. As the three trains of PSIS were activated, coolant was well injected at first. When the PBL was all full of steam and the top of the CMT was just starting to be filled with steam, the coolant injection through the CMT suddenly dropped and coolant was barely injected compared to the experiment. When the water temperature of the upper volume is heated after a long period, the injection was started again.

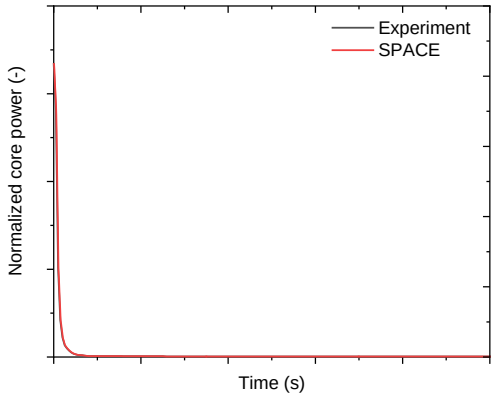

Fig. 6. Normalized core power after reactor trip (F101).

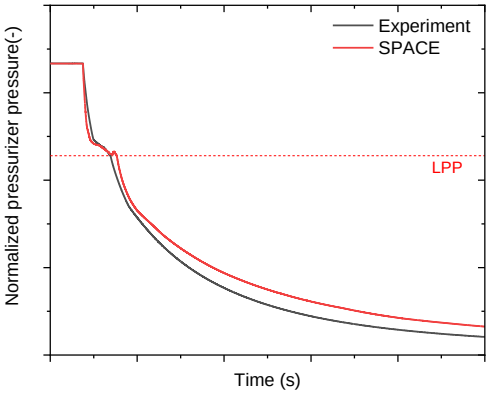

Fig. 7. Normalized pressurizer pressure (F101).

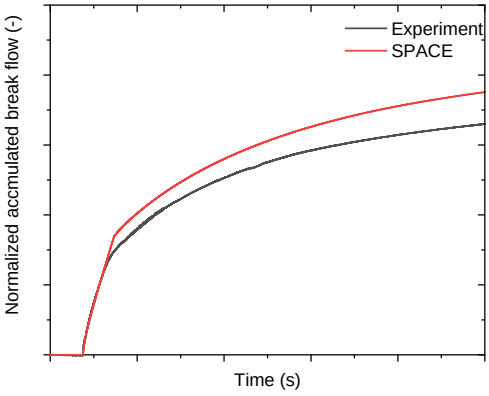

Fig. 8. Normalized accumulated break flow (F101).

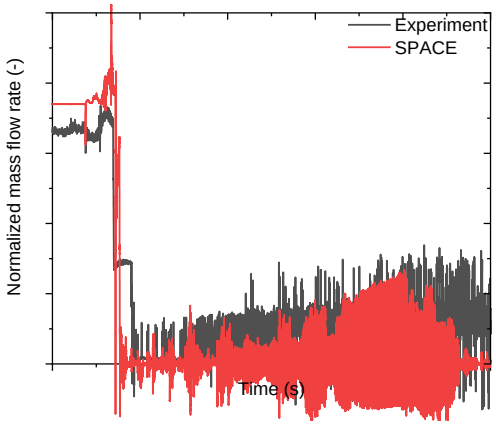

Fig. 9. Normalized RCS mass flow rate (F101).

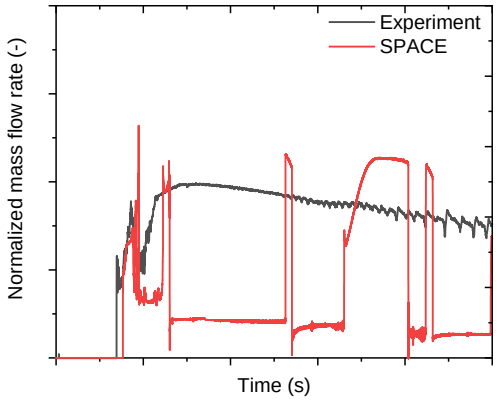

Fig. 10. Normalized PSIS #1 injection mass flow rate from CMT (F101).

This behavior also happened in the F102 calculation. Figs 11 to 14 show the normalized power after reactor trip, pressurizer pressure, accumulated break flow, and PSIS injection mass flow rate. As the pressurizer pressure reached the SITAS set point, safety injection into RPV was started through SIT. However, when the top side of SIT was about to be filled with steam, the coolant injection suddenly dropped until the upper volume water temperature is heated enough.

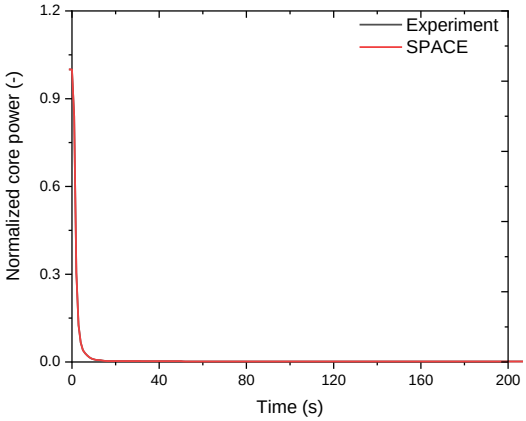

Fig. 11. Normalized core power after reactor trip (F102).

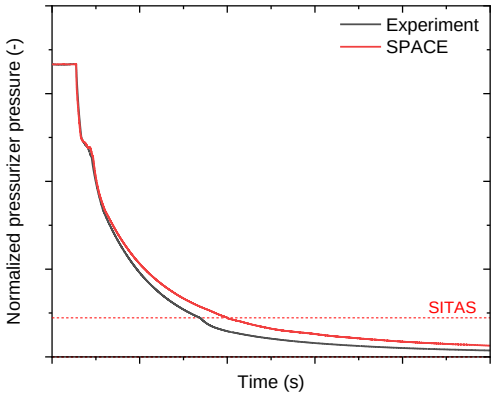

Fig. 12. Normalized pressurizer pressure (F102).

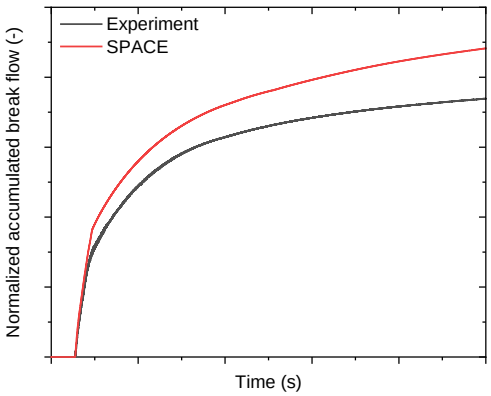

Fig. 13. Normalized accumulated break flow (F102).

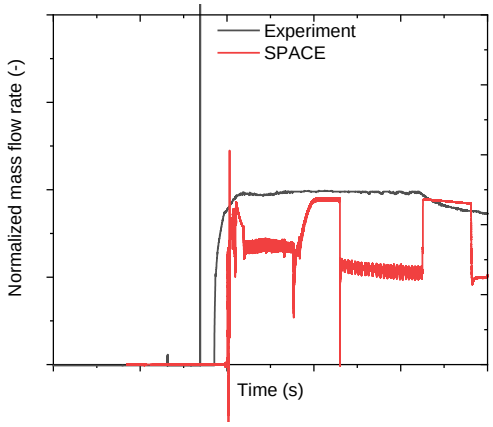

Fig. 14. Normalized PSIS #1 injection mass flow rate from SIT (F102).

This is because of the interfacial heat transfer in CMT and SIT. It is known that there are three phases in the PSIS operation: 1. Recirculation phase, 2. Oscillating phase, and 3. Injection phase [6]. Those phases are divided by major thermal-hydraulic phenomena. In the recirculation phase, because the PBL is filled with hot water, the density difference between the PBL and CMT creates the driving force. In the oscillating phase, 2-phase flow spills in the PBL and the density difference becomes larger. In the injection phase, the steam flows into the

CMT when the PBL is filled with steam and the stratified water is formed in the CMT. Fig. 15 shows the example of thermal-hydraulic phenomena in CMT and PBL.

In the calculations, PSIS injection dropped when the PSIS reached phase which means there is interfacial heat transfer in the CMT and SIT. In the experiment, a thermal layer is formed on the top of the water when steam is introduced into the top side of the CMT and SIT [5]. However, the SPACE code uses the bulk liquid temperature to calculate the interfacial heat transfer between the liquid phase and the interface. The subcooled water temperatures of the CMT and SIT are very lower compared to the steam temperature, so the interfacial heat transfer is very over-predicted, resulting in abnormal behaviors. Figs. 16 and 17 show the calculated water temperature behaviors in the CMT and SIT volume each. Comparing with Figs. 10 and 14, the PSIS injection is not performed until each of water in the volume is heated enough.

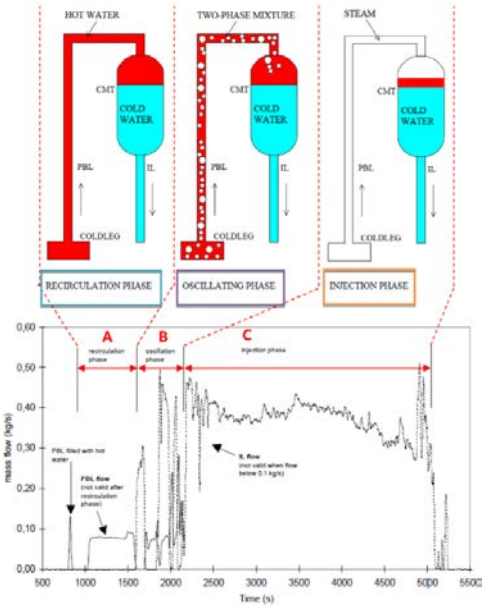

Fig. 15. Thermal-hydraulic phenomena in CMT and PBL on ALWR [6].

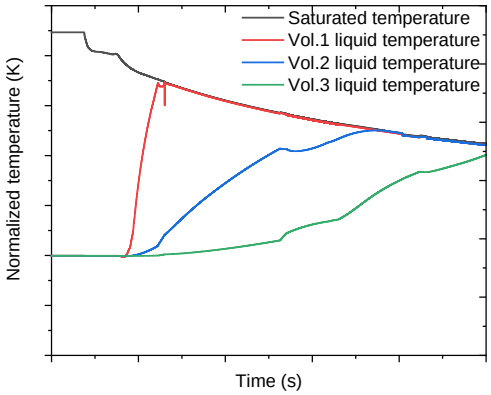

Fig. 16. Normalized CMT liquid temperature behavior in the F101 calculation.

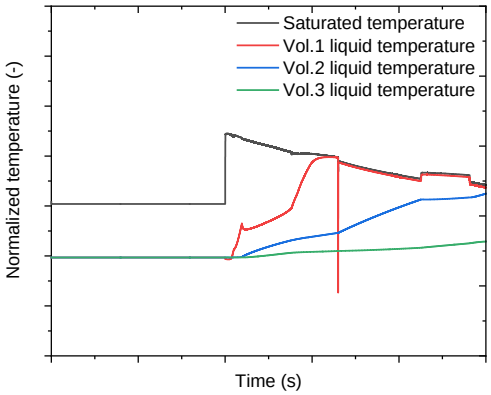

Fig. 17. Normalized SIT liquid temperature behavior in the F102 calculation.

We performed calculations by varying the number of nodes in the CMT and SIT. Figs. 18 and 19 show the calculated PSIS injection flow rates in each F101 and F102 calculations, varying CMT and SIT nodes. As shown in Figs. 18 and 19, discontinue interval becomes shorter as the number of nodes increases because the time to heat up the liquid in the upper volume becomes shorter. These behaviors are clearly shown in Fig. 20. Fig. 20 shows the CMT water level for each CMT node. However, the exact behavior of the PSIS cannot be predicted by increasing nodes. PNU derived the need for a CMT model development from the calculation results.

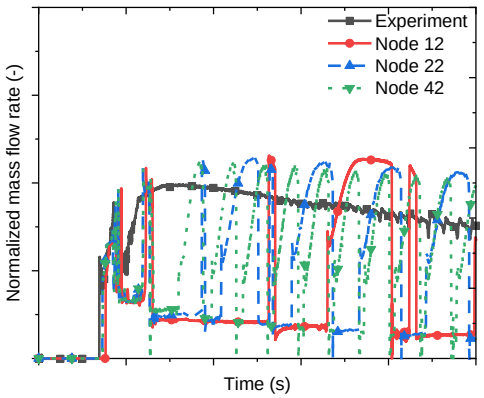

Fig. 18. Sensitivity calculation result about PSIS injection varying CMT nodes (F101).

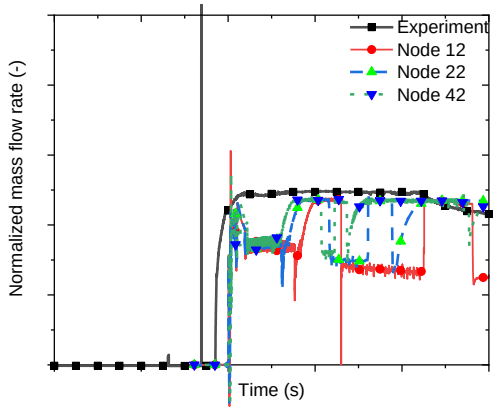

Fig. 19. Sensitivity calculation result about PSIS injection varying SIT nodes (F102).

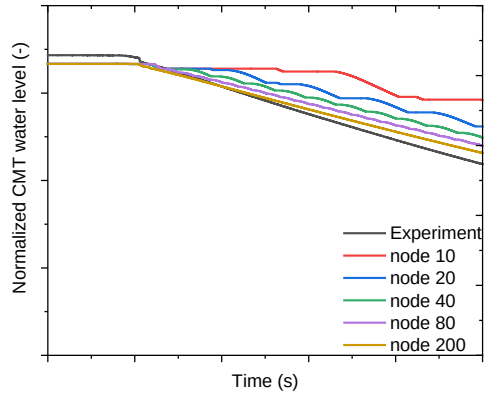

Fig. 20. Sensitivity calculation result about CMT water level varying CMT nodes (F101).

3. CMT model development and assessment

3.1 CMT model

In the SPACE code, the liquid energy conservation is as follows [7]:

$$V_{vol}^{n}\frac{\alpha_l^{n+1}\rho_l^{n+1}e_l^{n+1}}{\Delta t}+\sum\dot{\alpha}_l^{n}\dot{\rho}_l^{n}\dot{e}_l^{n}(\dot{u}_l^{n+1}A)+p^{n}\sum\dot{\alpha}_l^{n}\dot{u}_l^{n+1}A$$
$$=V_{vol}^{n}\left[-p^{n}\frac{\alpha_l^{n+1}-\alpha_l^{n}}{\Delta t}+Q_{il}^{n+1}-\Gamma_l^{n+1}h_l^{*}-S_E^{n}h_l^{n}+S_D^{n}h_d^{n}-Q_{l-n}^{n+1}\right]$$
$$+V_{vol}^{n}(Q_{w,l}^{n}-\Gamma_{w,l}^{n}h_l^{n}+Q_{w,il}^{n}+Diss^{n}) \quad (1)$$

In this equation, each interfacial heat transfer term and interfacial mass transfer term is calculated as:

$$Q_{il}^{n+1}=H_{il}^{n}(T^{s}(p_v)^{n+1}-T_l^{n+1}) \quad (2)$$

$$\Gamma_l^{n+1}=-\frac{\frac{p_v^{n}}{p^{n}}H_{iv}(T^{s}(p_v)^{n+1}-T_v^{n+1})+H_{il}(T^{s}(p_v)^{n+1}-T_l^{n+1})}{(h_v^{n,*}-h_l^{n,*})} \quad (3)$$

For predictions of the CMT and SIT behavior, the liquid temperature at the interface should be considered realistically.

The CMT model is based on lumped parameter model. Fig. 21 shows the simplified temperature distribution of the CMT. For the development of the lumped parameter CMT model, we set five assumptions. First, there is vertical stratified flow in CMT. Second, there is thermal stratification on the water top side. Third, there is linear temperature distribution in the thermal layer. Fourth, the thermal layer thickness (E_{il}) has a constant length. Fifth, the subcooled liquid under the thermal layer has a constant temperature.

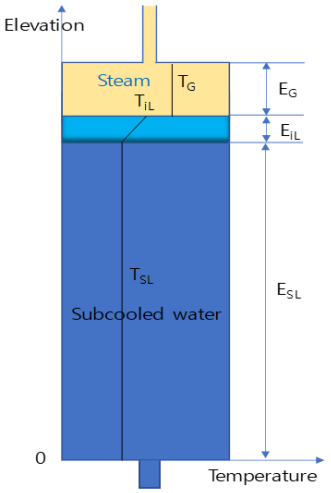

Fig. 21. Simplified CMT temperature distribution.

From these assumptions, each phase's portion (length) can be represented as:

$$E_g+E_{il}+E_{sl}=E_{CMT} \quad (4)$$

$$E_g=\alpha_g E_{CMT} \quad (5)$$

$$(E_{il}+E_{sl})T_l=E_{sl}T_{sl}+E_{sl}\frac{(T_{sl}+T_{il})}{2} \quad (6)$$

where

E_{il} is a thermal layer thickness.

E_g is a gas phase's length.

E_{sl} is a subcooled liquid phase's length.

T_{il} is liquid temperature at the interface.

T_{sl} is subcooled liquid temperature.

From Eq. (6), liquid temperature at the interface can be derived as:

$$T_{il} = \frac{2[(E_{il} + E_{sl})T_l - E_{sl}T_{sl}]}{E_{il}} - T_{sl} \quad (7)$$

Because each thermal layer thickness (E_{il}) and subcooled liquid temperature (T_{sl}) is assumed as a constant value, finally liquid temperature at the interface is as follows:

$$T_{il}^{n+1} = T_l^{n+1} + \left(1 + 2\frac{E_{sl}^n}{E_{il}}\right)(T_l^n - T_{sl}) \quad (8)$$

For the CMT component, the interface liquid temperature in Eq. (8) is replaced with the bulk liquid temperature for the interfacial heat and mass transfer terms in the SPACE code.

3.2 Assessment of CMT model

We implemented the CMT model into the SPACE code and calculated F101 and F102 tests. In this case, we modeled both CMT and SIT as a single cell using a cell component. Then, we compared the calculated PSIS injection between the CMT model with the original SPACE code.

Figs. 22 and 23 show PSIS injection mass flow rate in each F101 and F102 calculation. In both cases, the CMT model catches the safety injection behavior more reasonably. There is a sudden drop when water in the tank is empty but overall behavior is well predicted. Because the CMT and SIT are modeled as a single cell, water was not injected for a long time in the original SPACE code calculation.

In this paper, the heat structure was not attached to the CMT and SIT. To accurately calculate the effect on safety injection regarding the heat loss through PBL, CMT, and SIT, wall heat structure should be modelled.

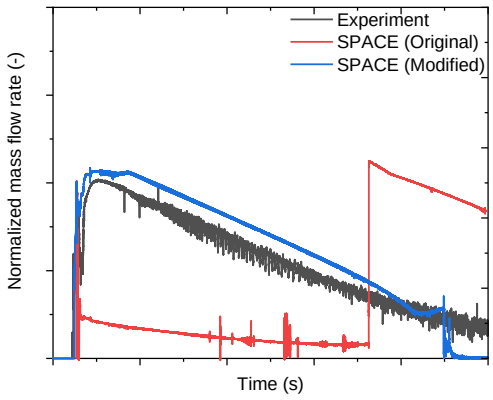

Fig. 22. Normalized PSIS #1 injection mass flow rate from SIT with the CMT model (F101).

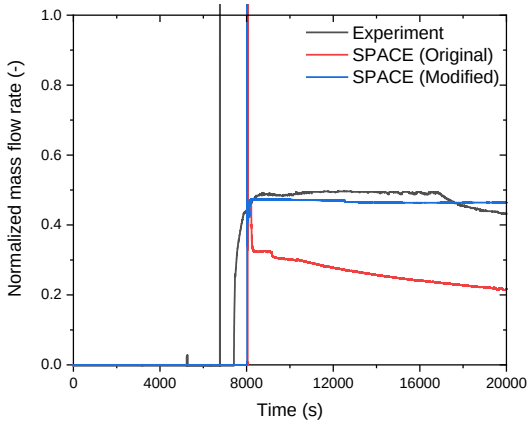

Fig. 23. Normalized PSIS #1 injection mass flow rate from SIT with the CMT model (F102)

3. Conclusions

In this paper, we simulated the PSIS performance tests of SMART-ITL. In general, the SPACE code over-predicted the interfacial heat transfer in the CMT and SIT. Thus, the SPACE code did not properly predict the PSIS injection behavior. To resolve this problem, we developed a lumped-parameter CMT model. Then, the CMT model was assessed using the SPACE code. It was shown that the CMT model predicts the behavior of the PSIS reasonably well when compared with the original SPACE code. For more accurate calculation, it is necessary to consider the wall heat transfer of the CMT and SIT.

ACKNOWLEDGEMENT

This research was supported by KAERI and King Abdullah City for Atomic and Renewable Energy (K.A.CARE), Kingdom of Saudi Arabia, within the Joint Research and Development Center.

REFERENCES

[1] K.K. Kim, W.J. Lee, S. Choi, H.R. Kim, and J.J. Ha, SMART: the first licensed advanced integral reactor, Journal of Power and Energy Engineering. 8, pp. 94– 102, 2014

[2] H.S. Park, H. Bae, S.U. Ryu, B.G. Jeon, J.H. Yang, Y.S. Kim, E.K. Yun, J.M. Kim, N.H. Choi, Y.C. Shin, K.H. Min, Y.G. Bang, M.J. Kim, C.J. Seo, and S.J. Yi, Core Cooling Behaviors in SMART-ITL with Passive Safety Injection System and Passive Residual Heat Removal System during a SBLOCA Scenario, Transactions of the Korean Nuclear Society Autumn Meeting, Gyeongju, Korea, May 18-19, 2017.

[3] H. S. Park, S. J. Yi, C. H. Song, SMR accident simulation in experimental test loop, Nuclear Engineering International, Nov. (2013) pp.12–15

[4] B.G. Jeon, Y.S. Cho, H. Bae, Y.S. Kim, S.U. Ryu, J.S. Suh, S.J. Yi, and H.S. Park, Code validation on a passive safety system test with the SMART-ITL facility, Journal of Nuclear Science and Technology, 54, pp. 322-329, 2017.

[5] H. Bae, S.U. Ryu, J.Y. Kang, J.H. Yang, Y.S. Kim, and H.S. Park, Data Analysis Report: 4-Train PSS tests, S-750-NV457-005, KAERI.

[6]. J. Tuunanen, J.Vihavainen, F. D'Auria, G. Kimber, Assessment of passive safety injection systems of ALWRs. In:

Final Report of the European Commission 4th Framework Programme, 1999.
[7] SPACE 2.13 Manual: Volume 1 Theory Manual, S06NX08-E-1-TR-11, KHNP, 2013. 06
[8] S.U. Ryu, H.B. Ryu, H.S. Park, and S.J. Yi, An experimental study on the thermal-hydraulic phenomena in the Hybrid Safety Injection Tank using a separate effect test facility. Annals of Nuclear Energy, 92, pp. 211-227, 2016